Check for updates

Synthesis and evaluation of new heteroaryl nitrones with spin trap properties†

G. Barriga-González, [ID] *[a] C. Aliaga, [ID] [bc] E. Chamorro, [ID] [d] C. Olea-Azar,[e] E. Norambuena,[a] W. Porcal,[f] M. González[f] and H. Cerecetto [ID] [f]

A new series of heteroaryl nitrones were synthesized and evaluated as free radical traps due to the results showed in our previous report. The physicochemical characterization of these new nitrones by electron spin resonance (ESR) demonstrated their high capability to trap and stabilize different atom centered free radicals generated by the Fenton reaction. Additionally, we intensely studied them in terms of their physicochemical properties. Kinetic studies, including the use of a method based on competition and the hydroxyl adduct decay, gave the corresponding rate constants and half-lives at the physiological pH of these newly synthesized nitrones. New nitrones derived from quinoxaline 1,4-dioxide heterocycles were more suitable than DMPO to trap hydroxyl free radicals with a half-life longer than two hours. We explain some of the results using computational chemistry through density functional theory (DFT).

Introduction

Due to natural metabolic activity in the human body, some of the essential by-products found are reactive oxygen and nitrogen species,[1,2] which mediate various physiological oxidative processes. The ability to reliably identify and quantify such short-lived oxidant species is critical to determine their role in human disease. In the past three decades, spin trapping, in conjunction with electron spin resonance spectrometry (ESR), has proven to be an essential experimental technique to accomplish this goal. In the last years, the spin-trapping technique was used to deeply study the behavior and role played by oxygen and nitrogen centered free radicals.[3,4] The most widely used spin trap has been the non-cyclic nitrones α-phenyl-*N-t*-butylnitrone and α-4-pyridyl-1-oxide-*N-t*-butylnitrone (PBN and POBN, respectively, Fig. 1A) and the cyclic one 5,5-dimethylpyrroline-*N*-oxide (DMPO, Fig. 1B).[5–8] In general terms, these available spin traps present many disadvantages such as low water solubility (in the case of PBN), sensitivity to nucleophilic

attack or other degradation reactions, and low stability of the generated spin adduct. Some new spin traps with better trapping abilities like BMPO, EMPO, and DEPMPO (Fig. 1B)[9,10] have been developed. However, despite the efforts, there are still limitations in their employment. In the past years, we found significant advances in the development of new free radical spin traps. Some new free radical spin traps, such as isoindole-based nitrones, have shown they can trap the nitric oxide radical (TMINO[11–13] and 3-TF-TMINO[14]).

We have described a new series of heteroaryl nitrones in previous work, bearing furoxanyl and thiadiazolyl moieties with the capability to trap and stabilize oxygen-, carbon-, sulfur-, and nitrogen-centered free radicals.[15] The spin trapping properties

[a]Departamento de Química, Facultad de Ciencias Básicas, Universidad Metropolitana de Ciencias de la Educación, Av. José Pedro Alessandri 774, Ñuñoa, Santiago, Chile. E-mail: german.barriga@umce.cl

[b]Facultad de Química y Biología, Universidad de Santiago de Chile, Av. Bernardo O'Higgins 3363, Santiago, Chile

[c]Centro para el Desarrollo de la Nanociencia y la Nanotecnología, CEDENNA, Chile

[d]Departamento de Ciencias Químicas, Facultad de Ciencias Exactas, Universidad Andrés Bello, Avenida República 275, 8370146 Santiago, Chile

[e]Departamento de Química Inorgánica y Analítica, Facultad de Ciencias Químicas y Farmacéuticas, Universidad de Chile, Santiago, Chile

[f]Grupo de Química Orgánica Medicinal, Laboratorio de Química Orgánica, Facultad de Ciencias/Facultad de Química, Universidad de la República, Montevideo, Uruguay

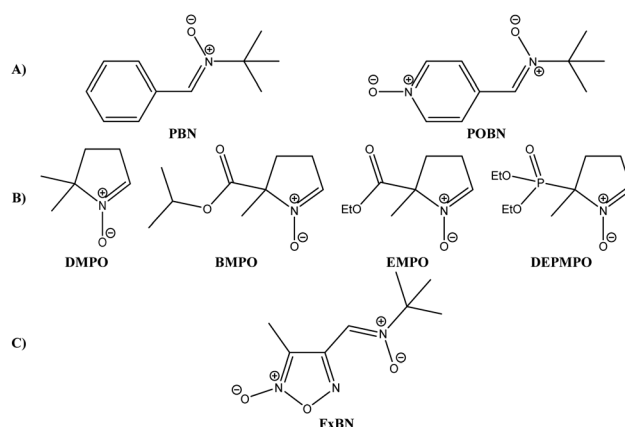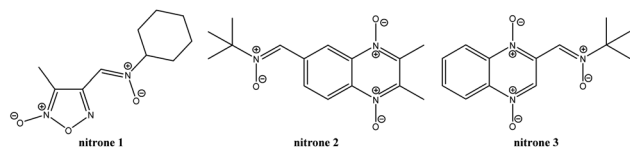† Electronic supplementary information (ESI) available. See DOI: 10.1039/d0ra07720h

Fig. 1 Structures of most used nitrones as spin trap agents today. (A) PBN and POBN, (B) DMPO, BMPO, EMPO, and DEPMPO, and (C) furoxanyl nitrone (**FxBN**) described by us.

Fig. 2 Structures of the heteroaryl nitrones described in the present work.

of the nitrones depends in great part on the connectivity and the nature of substituents on the nitrone group. As part of our ongoing investigations in the development of new nitrone-free radical trapping, we set out to design and synthesizer new heteroarylnitrones starting from suitable precursors available in our heterocyclic library. Notably, the 4-furoxanyl nitrone **FxBN** (Fig. 1C) showed good solubility in aqueous solution, and **FxBN** adducts formed with hydroxyl and superoxide radicals exhibited distinct and characteristic ESR spectral patterns.

Herein, we study and assay the spin trapping capabilities of three new heteroaryl nitrones (**nitrone 1**, **nitrone 2**, and **nitrone 3**, Fig. 2) against oxygen-, carbon-, sulfur-, and nitrogen-centered free radicals, *i.e.*, hydroxyl-, superoxide-, 1-hydroxyethyl-, methyl-, sulfur trioxide anion-, and azidyl-free radicals. Thus, kinetic constants and decay rates were obtained for the corresponding hydroxyl adduct at pH 7.4 in aqueous solution. Additionally, we performed assays for the trap of nitric oxide-free radicals and the behavior of these heteroaryl nitrones in biological models.

Experimental

Materials

The newly developed heteroaryl nitrones studied as spin traps are summarized in Fig. 2. 5,5-Dimethyl-1-pyrroline-*N*-oxide (DMPO, Fig. 1), dimethylsulfoxide, anhydrous sodium sulfite, monobasic potassium phosphate, sodium hydroxide, *N*-methyl-D-glucamine (MGD), diethylenetriaminepentaacetic acid, xanthine, and xanthine oxidase were purchased from Sigma-Aldrich. Sodium azide, hydrogen peroxide aqueous solution (30%), anhydrous ethanol, dibasic sodium phosphate heptahydrate, methanol, carbon disulfide, and sodium nitrite were purchased from Merck. Ferrous ammonium sulfate hexahydrate was purchased from Mallinckrodt Baker.

Synthesis

Before using, all solvents were distilled, and experimental conditions for analytical TLC and column chromatography purification was used according to previous work. The electrothermal 9100 apparatus was used to determining melting points, and they are uncorrected. Microanalyses were performed on a Fisons EA 1108 CHNS-O instrument and were within ±0.4% of the calculated compositions. Bruker DPX-400 spectrometer was used to record NMR spectra. The assignment of chemical shifts is based on standard NMR experiments (^{1}H, ^{13}C, ^{1}H-COSY, HSQC, HMBC, and NOE). The chemical shift values are expressed in ppm relative to tetramethylsilane as an

internal standard. Shimadzu DI-2010 was used to determine the mass spectra.

2-Formylquinoxaline 1,4-di-*N*-oxide (V). A mixture of SeO$_2$ (0.09 g, 0.80 mmol) in dioxane (5 mL)/H$_2$O (0.1 mL) was heated at reflux. Then 2-methylquinoxaline 1,4-di-*N*-oxide (**IV**) (0.1 g, 0.57 mmol) was added, and the final mixture was stirred for two hours. The resulting dispersion was then filtered through a short pad of Celite, the organic phase concentrated *in vacuo*, and the residue purified by column chromatography (SiO$_2$, AcOEt), yielding derivative **V** as a yellow solid (100 mg, 86%). ^{1}H-NMR (CDCl$_3$) δ: 8.00 (m, 2H), 8.64 (s, 1H), 8.69 (m, 2H), 10.65 (s, 1H).

Synthetic procedure of α-heteroaryl-*N*-alkylnitrone derivatives (1–3). A mixture of the corresponding aldehyde (1.0 equivalent), *N*-alkylhydroxylamine hydrochloride or the corresponding acetate (1.2 equivalent), and sodium bicarbonate (1.2 equivalent) in absolute ethanol (5 mL mmol^{-1}) as solvent was heated at 60 °C until the carbonyl compound was not present (checked by TLC). The solvent was removed *in vacuo*, and the residue was purified by column chromatography (SiO$_2$, mixtures of petroleum ether/EtOAc).

α(Z)-(3-Methylfuroxan-4-yl)-*N*-cyclohexylnitrone (1). Pale yellow solid (60%); mp 118.0–120.0 °C. Found: C, 52.9; H, 6.5; N, 18.6. C$_{10}$H$_{15}$N$_3$O$_3$ requires C, 53.3; H, 6.7; N, 18.7. ^{1}H-NMR (CDCl$_3$) δ: 1.21 (m, 1H, CH), 1.40 (m, 2H, CH$_2$), 1.73 (m, 1H, CH), 1.95 (m, 4H, CH$_2$), 2.15 (m, 2H, CH$_2$), 2.41 (s, 3H, CH$_3$), 4.01 (m, 1H, CH–N), 7.57 (s, 1H, CH=N). ^{13}C-NMR (CDCl$_3$) δ: 10.3 (<u>C</u>H$_3$), 24.9 (cyclohexyl-<u>C</u>H$_2$), 25.1 (cyclohexyl-<u>C</u>H$_2$), 31.2 (cyclohexyl-<u>C</u>H$_2$), 76.1 (cyclohexyl-<u>C</u>H), 112.5 (furoxanyl-<u>C</u>=N→O), 119.8 (nitrone-<u>C</u>H=N→O), 150.6 (furoxanyl-<u>C</u>=N). ESI-MS, *m/z*: 248 (M$^{+\bullet}$ + Na), 226 (M$^{+\bullet}$ + H), 144, 100.

α(Z)-(1,4-Dioxide-2,3-dimethylquinoxalin-6-yl)-*N*-t-butylnitrone (2). Yellow solid (35%); mp 209.4–212.3 °C. Found: C, 62.0; H, 6.7; N, 14.3. C$_{15}$H$_{19}$N$_3$O$_3$ requires C, 62.3; H, 6.6; N, 14.5. ^{1}H-NMR (CDCl$_3$) δ: 1.67 (s, 9H, (CH$_3$)$_3$C), 2.75 (s, 6H, CH$_3$), 7.85 (s, 1H, quinoxalinyl-C$_5$H), 8.62 (d, 1H, J = 8.8 Hz, quinoxalinyl-C$_7$H), 9.03 (d, 1H, J = 8.8 Hz, quinoxalinyl-C$_8$H), 9.13 (s, 1H, CH=N). ^{13}C-NMR (CDCl$_3$) δ: 14.7 (<u>C</u>H$_3$-quinoxalinyl), 28.4 ((<u>C</u>H$_3$)$_3$C), 72.3 ((CH$_3$)$_3$<u>C</u>), 119.7 (nitrone-<u>C</u>H=N→O), 120.4 (quinoxalinyl-<u>C</u>=N→O), 128.2 (quinoxalinyl 7-C), 130.5 (quinoxalinyl 6-C), 130.6 (quinoxalinyl 5-C), 133.9 (quinoxalinyl 8-C), 136.3 (quinoxalinyl quaternary-C), 141.6 (quinoxalinyl quaternary-C). EI-MS *m/z* (%): 289 (M$^{+\bullet}$, 83), 273 (21), 257 (4), 233 (100), 216 (86), 199 (33).

α(Z)-(1,4-Dioxidequinoxalin-2-yl)-*N*-t-butylnitrone (3). Yellow solid (95%); mp 191.8–193.5 °C. Found: C, 59.6; H, 5.9; N, 15.8. C$_{10}$H$_{15}$N$_3$O$_3$ requires C, 59.8; H, 5.8; N, 16.1. ^{1}H-NMR (CDCl$_3$) δ: 1.67 (s, 9H, (CH$_3$)$_3$C), 7.86 (m, 2H, quinoxalinyl-C$_6$H and quinoxalinyl-C$_7$H), 8.61 (m, 2H, quinoxalinyl-C$_5$H and quinoxalinyl-C$_8$H), 8.70 (s, 1H, quinoxalinyl-C$_3$H), 10.30 (s, 1H, CH=N). ^{13}C-NMR (CDCl$_3$) δ: 28.3 ((<u>C</u>H$_3$)$_3$C), 74.4 ((CH$_3$)$_3$<u>C</u>), 119.8 (nitrone-<u>C</u>H=N→O), 120.3 (quinoxalinyl-<u>C</u>=N→O), 120.6 (quinoxalinyl-<u>C</u>=N→O), 129.9 (quinoxalinyl 6-C and quinoxalinyl 7-C), 131.6 (quinoxalinyl 8-C), 132.2 (quinoxalinyl 5-C), 135.8 (quinoxalinyl quaternary-C), 137.6 (quinoxalinyl quaternary-C). EI-MS *m/z* (%): 261 (M$^{+\bullet}$, 23), 245 (13), 205 (19), 189 (37), 172 (35), 129 (26), 105 (24), 57 (100).

Free radical generation and ESR measurements

Radicals were generated by employing a Fenton type reaction. Aqueous solutions of Fe^{2+} (1.0 mM of ferrous ammonium sulfate hexahydrate) and hydrogen peroxide (1%) in phosphate buffer (pH 7.4) was loaded into the ESR cell. Thus, for 1-hydroxyethyl, methyl, sulfur trioxide anion, and azidyl radicals, we employed as generation source the following reactants: anhydrous ethanol (200 mM), anhydrous dimethylsulfoxide (200 mM), anhydrous sodium sulfite (200 mM), and anhydrous sodium azide (200 mM), respectively. POBN (50 mM) and DMPO (50 mM) were used as a control to check the generation of 1-hydroxyethyl, hydroxyl, and superoxide free radical, respectively.[16]

The xanthine/xanthine oxidase couple was used for superoxide anion radical, and the detection procedure was modified from literature[17] with the following conditions: the assayed nitrone (50 mM) was incubated with xanthine (0.4 mM) and xanthine oxidase (0.06 units per mL) in phosphate-buffered saline (PBS, 100 mM, pH 7.4, containing 1.0 mM DTPA). In order to verify the proper generation of superoxide anion free radical, DMPO was used as spin trap control.

The following procedure was used for nitric oxide radical generation: MDG (50 mM),[18] Fe^{2+} (10 mM), $NaNO_2$ (100 mM), and the corresponding nitrone (50 mM). In order to verify the proper generation of nitric oxide free radical, MGD–Fe^{2+} complex was used as spin trap control.

Bruker ECS 106 ESR (X-band) spectrometer equipped with a rectangular cavity was used to record the ESR spectra at room temperature. The spectrometer conditions were microwave frequency, 9.80 GHz; modulation frequency, 50 kHz; microwave power, 20 mW; modulation amplitude, 0.9 G; time constant, 81.92 ms; the number of scans, 12.
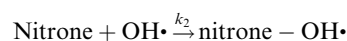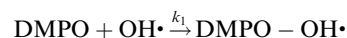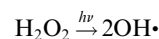
ESR simulation

The NIEHS WinSim software was used for the ESR spectra simulation.[19] The simulations of the spectra give us a systematic study based on the dependencies of certain spectral features with some magnetic parameters and accurate parameter extraction from obtained experimental data.

Rate constant and half-life estimation for ·nitrone–OH adduct

The measure of the decay constant for the nitrone–hydroxyl adduct used the same procedure described above for the generation of hydroxyl radical *via* Fenton reaction. Following the decrease of an appropriate ESR line was used to monitoring the decay of the spin adduct.[20,21] Pseudo-first-order decay of the spin adduct was measured by continuously recording the ESR signal intensity. Although the decay of a spin adduct should follow second-order kinetics, under the experimental conditions used in the present work, it can be treated as pseudo-first-order due to the spin trap concentration used. This was in a significant excess compared to the radical concentration and making us consider the concentration of radical trapping constant throughout the experiment. The only variable that changes through the duration of the experiment was the

concentration of the generated free radical species. The decay rate was also calculated from the double integral of the ESR spectra. Therefore, it may differ from the rate calculated from the concentration. The relative spin trapping rate for hydroxyl radical was determined using a competitive-trapping method.[21] In this method, two spin traps are mixed (DMPO and nitrones studied), and the ESR signal intensities are compared using the value of the double integral of the recorded spectra. The reaction scheme for spin trapping in the competition method for the hydroxyl radical with both spin traps compounds is:

$$H_2O_2 \xrightarrow{h\nu} 2OH\bullet$$

$$DMPO + OH\bullet \xrightarrow{k_1} DMPO - OH\bullet$$

$$Nitrone + OH\bullet \xrightarrow{k_2} nitrone - OH\bullet$$

First, we assumed first-order rates for the formation of the two spin adducts, and the intensities found can be related as follows:

$$\frac{I_{DMPO}}{I_{nitrone}} = \frac{k_{1DMPO}}{k_{2nitrone}}$$

The value of k_{DMPO} has been previously determined.[22]

Spin trapping in biological systems studies

The spin trap capability of the new nitrones was assessed in mouse mammary adenocarcinoma TA3 cell line exposed to 5-nitroindazole, a free radical producer agent. ESR spectra were obtained using the following conditions: studied nitrones (50 mM), mouse mammary adenocarcinoma TA3 cells (4.0 mg mL^{-1}), and 5-nitroindazole (25 mM), in phosphate buffer, pH 7.4. The mixture was transferred to a 100 μL capillary. A Bruker ECS 106 spectrometer (rectangular cavity and 50 kHz field modulation) was used to record ESR spectra at the X band (9.80 GHz). After 12 scans, all the spectra were registered on the same scale.[23]

Computational calculations

In order to explain results obtained in the trapping of the other radicals using these new heteroaryl nitrones, we used Density Functional Theory (DFT)[24,25] calculations using Jaguar software.[26] We used the B3LYP/6-31++G** level for optimization of the geometries and to obtain the spin density isosurfaces. Solvent effects were investigated using the polarizable continuum model (PCM).[27–29]

Results and discussion

The previous results with the furoxanyl nitrone **FxBN** (Fig. 1C) conduct us to use it as a basic template to produce new analogs with modified physicochemical properties. In this sense, in order to study the stability of the generated spin adduct, we designed and synthesized **nitrone 1** (Fig. 2), where **FxBN** *t*-butyl
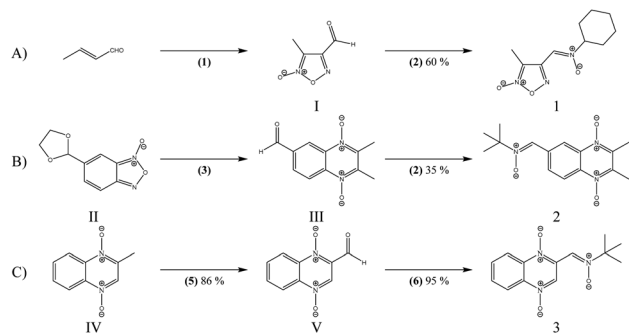
Scheme 1 Synthesis of heteroarylnitrones **1–3**. Experimental conditions are: (A) (**1**) NaNO$_2$/AcOH, (**2**) C$_6$H$_{11}$−NHOH·HCl/NaHCO$_3$/EtOH/60 °C. (B) (**3**) (i) butanone/NH$_3$ (g), (ii) HCl (c), (**4**) (CH$_3$)$_3$−NHOH·AcOH/NaHCO$_3$/EtOH/60 °C. (C) (**5**) SeO$_2$/dioxane/H$_2$O/reflux, (**6**) (CH$_3$)$_3$C−NHOH·HAc/NaHCO$_3$/EtOH/60 °C.

Fig. 3 (A) The left spectrum corresponds to the trap of 1-hydroxyethyl radical, **nitrone 1** was used as a spin trap. The center spectrum showed the hyperfine splitting pattern for the trap of sulfur trioxide anion radical when **nitrone 2** was used. It is possible to observe some minor artifacts in the spectra. The right spectrum is **nitrone 3** trapping azidyl radical. (B) Experimental spectra are shown in blue, and the corresponding simulations are remarked with red color. From left to right, simulations of the trap of methyl, hydroxyl, and azidyl radical with **nitrones 1**, **2**, and **3**, respectively.

moiety was substituted by a cyclohexyl group. On the other hand, due to **FxBN** possesses a cyclic nitrone group in the furoxanyl ring, we aimed to analyze the effect of other nitrone containing cyclic N-oxides. To do this, we selected the well-known quinoxaline 1,4-dioxide heterocycle, which involves two cyclic-nitrone moieties, and additionally, we selected two different positions for the non-cyclic extra nitrone (**nitrone 2**, and **nitrone 3**, Fig. 2). The different non-cyclic nitrone positions and substituents on the quinoxaline nucleus could modify the physicochemical properties of these compounds.

The new nitrones were synthesized through the condensation between heteroaromatic aldehydes and N-t-butylhydroxylamine or N-cyclohexylhydroxylamine with moderate to excellent yields (Scheme 1).[30]

The formylfuroxan **I** was obtained from crotonaldehyde through reaction with NaNO$_2$ in AcOH by intramolecular cyclization (Scheme 1A).[30] We employed the synthetic route showed in Scheme 1B to obtain the desired formylquinoxaline 1,4-dioxide **III**. Beirut reaction of bezofuroxan **II** with butanone in the presence of NH$_3$ (g) gave the compound **III** in good yield.[31] Using the Beirut reaction, the 2-methylquinoxaline 1,4-di-N-oxide intermediate **IV** (Scheme 1C) was synthesized, from benzofuroxan reacting with acetone in the presence of pyrrolidine.[32] Then we proceeded to the oxidation of the methyl group in position 2 of the quinoxaline ring, using SeO$_2$ as the oxidant agent in order to obtain the carboxaldehyde derivative **V**. Finally, the desired heteroaryl nitrones, **1–3**, were obtained for the reaction between the corresponding aldehydes **I**, **III**, **V** and N-substituted hydroxylamine in the presence of NaHCO$_3$ (Scheme 1).

Spin trapping assays

Firstly, the spin trapping properties of these new nitrones were investigated against different centered free radicals (O, C, N, and S atoms, respectively). The radicals generated were hydroxyl, 1-hydroxyethyl, azidyl, and sulfur trioxide anion. All radicals mentioned above were generated through Fenton's reagents, using aqueous solutions of Fe^{2+} and hydrogen peroxide (1%), ethanol, sodium azide, or sodium sulfite, respectively.
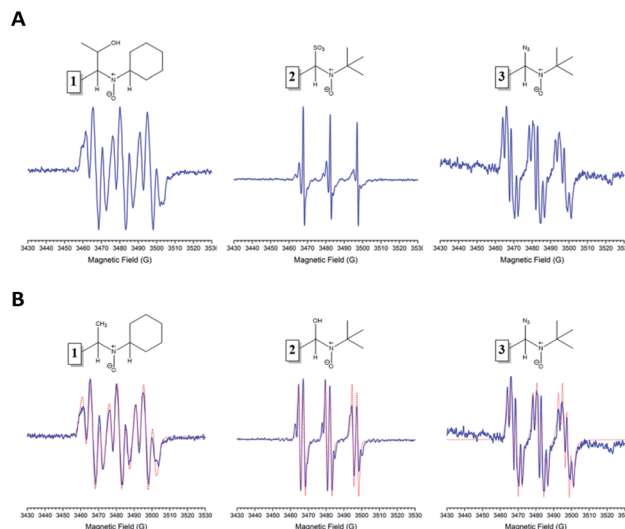
Each of the nitrones tested gave an ESR-detectable spin adduct with other radicals (Fig. 3A and B).

The obtained spin adducts spectrum was composed as follows: for hydroxyl and 1-hydroxyethyl radicals, the pattern obtained was composed of six-line (triplet of doublet) due to coupling of the unpaired electron with nitrogen and hydrogen at α-carbon, except for **nitrone 1**, which the obtained pattern was composed by nine lines (triplet of triplet, Fig. 3A) probably due to the extra hydrogen located in the cyclohexyl moiety. In order to explain this different behavior, we proceeded to perform the corresponding computational calculations using DFT level, explaining the hyperfine pattern found. From the analysis of the spectrum, it was obtained that a second H atom with a smaller hyperfine coupling constant would explain the observed hyperfine pattern. The spin density reveals that this is
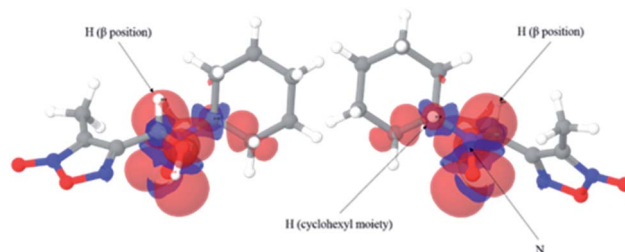

Fig. 4 Spin density isosurface for **·nitrone 1**−OH spin adduct using DFT calculus. The arrows indicate the atoms in which the unpaired electron is delocalized and forms the hyperfine pattern are observed experimentally.

delocalized to a part of the cyclohexyl group. Fig. 4 shows the atoms contributing to the hyperfine pattern found, confirming that this substituent group influences the spectrum pattern.

The ESR spectrum when methyl radical was trapped was composed of a triplet of doublet due to coupling with a nitrogen atom (triplet) and β-hydrogen atom (doublet) at the α-carbon atom, except for **nitrone 1** (Fig. 3B). The ESR spectrum for **nitrone 1** trapping methyl radical was composed again by nine lines. The spin adducts with the azidyl radical exhibit twelve-line (Fig. 3A and B) attributed to a triplet of triplet of doublets. This pattern is explained due to two different nitrogen atoms, one atom from the nitrone group and the other atom from the azidyl radical. To complete the pattern explanation, we considered the contribution of the β-hydrogen atom to this splitting. For **nitrone 1**, the intensity of the signal is weak, and the spectrum is not well resolved. Finally, the spin trapping properties of these new nitrones were investigated against sulfur-centered free radical produced by sulfur trioxide anion free radical. The spin adducts from these nitrones showed symmetrical patterns in all the cases. The ESR spectrum for **nitrone 1** was composed of nine lines (triplet of triplet). For **nitrones 2** and **3**, the hyperfine pattern is similar, and it can be observed in the value of the hyperfine splitting constant (Fig. 3A). Fig. 3B showed the ESR simulations for all data correlated well with experimental ESR spectra.

Table 1 resumes the hyperfine constants coupling for the different generated spin adducts.

In the case of **nitrones 2** and **3**, the nitrogen hyperfine constants between the trapping of the hydroxyl, methyl, 1-hydroxyethyl, and sulfite radical have the same values. For the hydrogen atom, these hyperfine constants showed a slight difference. It can be appreciated that **nitrone 1** has very different hyperfine coupling constants compared with **nitrones 2** and **3**. Among the other radicals trapped, the hyperfine splitting constant showed similar values for nitrogen atom and the same behavior for the two hydrogen atoms (except for azidyl radical).

Table 2 The half-life for **nitrones 1**, **2**, and **3**, PBN, DMPO, and **FxBN** with hydroxyl radical at pH 7.4.

Spin adduct	Half-life (s)
˙DMPO–OH	3300
˙PBN–OH	∼38
˙FxBN–OH	7567
˙Nitrone 1–OH	3398
˙Nitrone 2–OH	8923
˙Nitrone 3–OH	7270

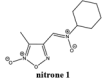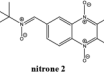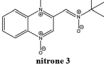### Determination of spin adduct stability and the decay rate constant for ˙nitrone–OH spin adducts

Regardless of this, all nitrones under study showed a behavior as spin traps. To get insight into the physicochemical properties of ˙nitrone–OH spin adducts, stability, and kinetic studies in PBS (pH = 7.4) were performed. The stability of spin adducts was studied through the monitoring of the disappearance of the ESR signal intensity of ˙nitrone–OH spin adducts (see example in Fig. 5a).

It could be attributed to a solvolysis process as the mechanism of decay.[7,33,34] The half-life of ˙nitrone–OH spin adduct was determined, assuming that the decay is of first-order. Both **nitrones 2** and **3** showed excellent stability with a $t_{1/2}$ more than 100-fold higher the value for ˙DMPO–OH adduct[3] (Table 2).

We also included the values for the previously reported **FxBN** nitrone[15]

Until this stage of experiments, we discussed some aspects concerning the structural characteristics of these new nitrones. First, unlike that, it was observed in our previous work furoxanyl substituent did not exert an excellent stabilizing effect in the trapped radicals as it happens with the **nitrone 1** (compare $t_{1/2}$ for ˙FxBN–OH and ˙nitrone 1–OH in Table 2). However, the use of a cyclohexyl substituent gives us the possibility to obtain

Table 1 Hyperfine constant coupling values of the different nitrones–radicals spin adducts and the corresponded g value

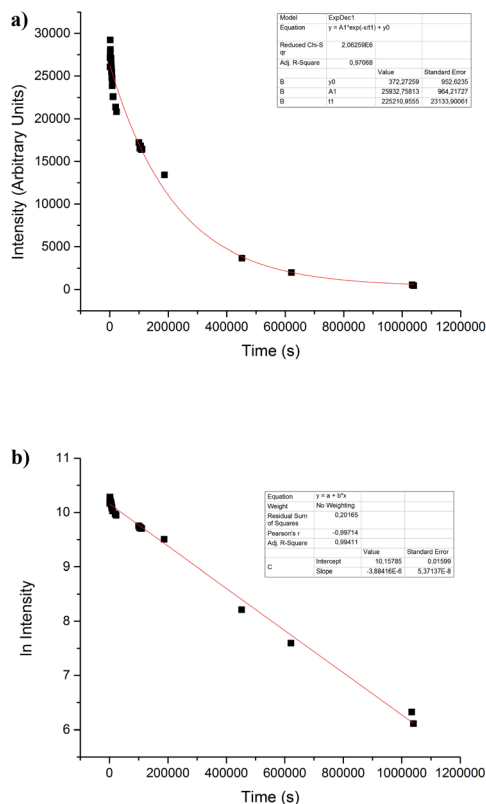|	˙CH$_3$			CH$_3$˙CHOH			˙N$_3$			˙OH			˙SO$_3^-$		
	a_N	a_H	a_H	a_N	a_H	a_H	a_N	a_N	a_H	a_N	a_H	a_H	a_N	a_H	a_H
nitrone 1	14.7	5.0	4.1	14.7	5.1	4.0	15.0	5.5	3.9	14.8	5.1	3.9	14.6	5.2	4.2
g value	2.00925			2.00919			2.01435			2.01119			2.01135		
nitrone 2	15.1	2.8	ns^a	15.5	3.1	ns	14.3	2.1	1.6	15.1	2.8	ns	15.0	1.9	ns
g value	2.00953			2.00702			2.00841			2.00879			2.00885		
nitrone 3	14.4	2.2	ns	14.4	2.1	ns	14.4	2.3	2.5	14.4	2.2	ns	14.5	2.0	ns
g value	2.00829			2.00863			2.00840			2.00846			2.00834		

^{a} No signal.

Fig. 5 (a) The time course of the ESR signal intensity for ˙nitrone 2–OH adduct, in PBS (pH = 7.4). The decay agrees with a first-order reaction. (b) The time course of the ESR signal intensity is expressed as the natural logarithm of intensity for ˙nitrone 2–OH adduct, confirming a process of first-order decay.

Table 3 Comparison and relationship of the constants for the trapping of hydroxyl radical. DMPO was used as a pattern

Nitrone	k_{ST} (dm³ mol⁻¹ s⁻¹)	k_2/k_1
DMPO	3.4×10^9	1.00
FxBN	1.22×10^{10}	3.59
Nitrone 1	1.17×10^9	0.34
Nitrone 2	1.70×10^{10}	5.00
Nitrone 3	1.61×10^{10}	4.74

a hyperfine pattern. Although it was similar in all cases, it was more sensitive to changes in the hyperfine coupling constants compared with *t*-butyl substituent used in the **nitrones 2** and **3**. Instead, the usage of a quinoxalinyl substituent conferred an essential aid in stabilizing the other radicals trapped (compare $t_{1/2}$ for ˙**FxBN**–OH and ˙**nitrone 2**–OH in Table 2). Probably this substituent imparts a planar structure that helps the electronic delocalization and the consequent stabilization of the corresponding spin adduct.

Competitive studies for ˙OH-trapping

We determined the ratio of constants through a competitive study, (k_2/k_1) of hydroxyl radical for the studied nitrones, the
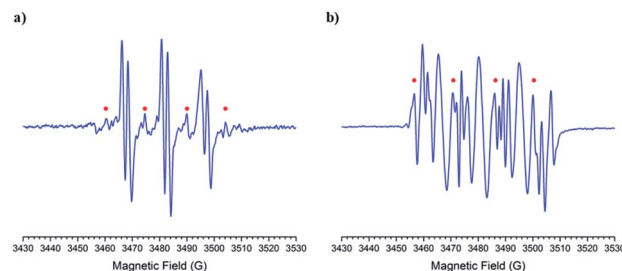

Fig. 6 ESR spectra obtained after the generation of hydroxyl radical using Fenton reaction, ˙DMPO–OH spin adduct, was marked with red dots. (a) **Nitrone 3** competitive spectrum obtained *versus* DMPO trapping hydroxyl radical. (b) **Nitrone 1** competitive spectrum obtained *versus* DMPO for the same radical mentioned above.
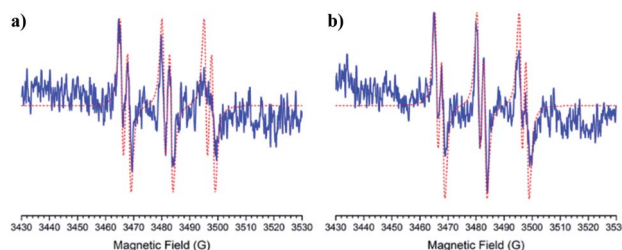

Fig. 7 Hyperfine patterns for the trapping of nitrogen dioxide radical (˙NO₂). (a) **Nitrone 2** spectrum of ˙NO₂ radical trapping process, in blue experimental results and in red the corresponding simulation. (b) The spectrum for **FxBN** trapping ˙NO₂ radical process, in blue experimental results and in red the corresponding simulation.

previously reported nitrone **FxBN** and DMPO (Table 3), being for DMPO $k_1 = 3.4 \times 10^9$ dm³ mol⁻¹ s⁻¹.[35]

It was possible to observe that **nitrone 2** and **3** exhibited the fastest rate in trapping hydroxyl radical when was compared with DMPO and the previously reported **FxBN** (see example in Fig. 7a and results in Table 3). However, when the same kind of competitive experiment was performed with **nitrone 1**, a slower trapping process compared to DMPO occurred (Fig. 6b and Table 3).

It could be correlated with the different structural moieties with the different reactivity and stability between these
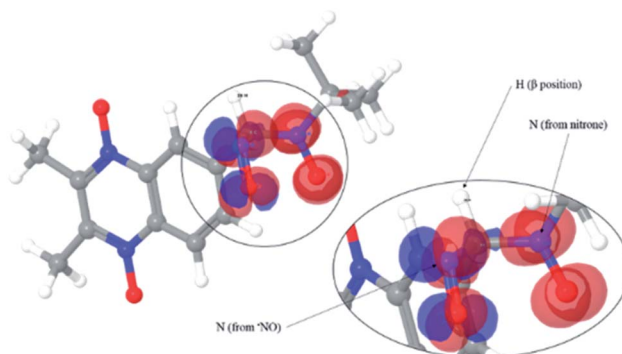

Fig. 8 Spin density isosurface for ˙**nitrone 2**–NO spin adduct using DFT.

Table 4 The hyperfine coupling constant for the trapping of nitrogen dioxide radicals

	$\cdot NO_2$	
	a_N	a_H
Nitrone 1	ns	ns
Nitrone 2	15.0	2.6
Nitrone 3	15.0	2.0
FxBN	15.0	2.3

nitrones[36] claiming the relevance of the quinoxaline 1,4-dioxide substructure on **nitrone** 2 and 3 in the spin adduct stabilization.

Trapping of nitric oxide and superoxide anion radicals

Nitric oxide (NO) is a signaling and regulatory molecule in many physiological and pathological processes.[37] Several attempts have been performed to detect NO in aqueous solutions and biological systems by using spin trapping methodology.[38] However, the traditional nitrone spin traps such as PBN and DMPO appeared to be unsuitable as they did not form stable and characteristic spin adducts with NO.[38] These limitations suggest the need to develop new spin trapping agents, which can specifically trap NO generated under physiological conditions. In this context, the ability of the newly synthesized nitrones to trap the nitric oxide radical was studied. Thus, we performed the same test with the **FxBN** nitrone, in which it was clear that it can trap the $\cdot NO_2$ radical (Fig. 7).

The analysis of the intensities of the lines by double integration allows us to point out that the **nitrone 2** is better compared to **FxBN**.

The spectra obtained were composed of six lines (triplet of doublet) for **nitrones 2** and **3**. **FxBN** nitrone exhibited the same spectrum as described above. Because the obtained pattern was not than expected, computational calculations were performed in order to determine the trapped species. Structures were optimized for **nitrones 2** and **3**, simulating the trapping of NO and $\cdot NO_2$ free radicals. If the nitrones trap NO free radical
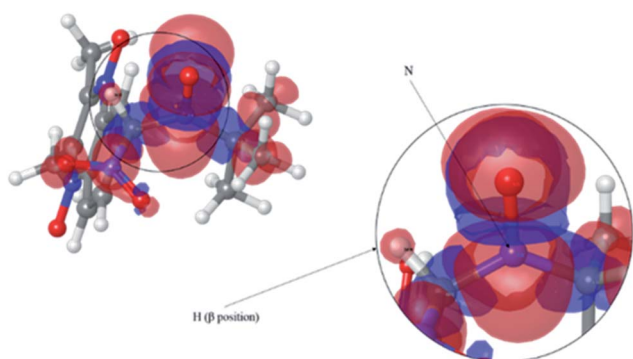

Fig. 10 ESR spectra for the $\cdot$nitrone–OOH adducts were obtained with **nitrone 2** (left) and **nitrone 3** (right).

Table 5 Hyperfine splitting for the trap of superoxide anion radical with studied nitrones

	$\cdot O_2{}^-$		
	a_N	a_H	a_H
Nitrone 1	ns	ns	ns
Nitrone 2	15.3	2.9	ns
Nitrone 3	15.3	2.0	ns
FxBN	15.6	1.9	1.2

(Fig. 8 for **nitrone** 2), according to the calculus, it should be observed a hyperfine pattern composed by two nitrogen atoms, one from the trapped radical and the other from the nitrone group, with no signal being observed for the β-position hydrogen (Table 4).

The isosurface showed that the spin density is mainly located on each of the mentioned nitrogen atoms.

When we performed the same analysis using $\cdot NO_2$ as trapped free radical, it was observed that the spin density was primarily located between the nitrogen and hydrogen in the β-position of the nitrone group (Fig. 9).

This result showed that the observed spectra would correspond to a triplet of doublet as observed in experimental spectra (Fig. 7) with some minor influences from the nitrogen atom from the nitrogen dioxide radical. Therefore, under the conditions in which was generated the NO radical, these nitrones are not capable of trapping the NO free radical in contrast to that occurs when using the complex MGD–Fe^{2+} as spin traps.

For the generation of superoxide anion radical was used as the system xanthine/xanthine oxidase. The results showed that

Fig. 9 Spin density isosurface for $\cdot$**nitrone 2**–NO_2 spin adduct using DFT calculus. In this model, we could corroborate that the nitrones were not capable of trapping nitric oxide radical, and the experimental spectra corresponded to the trap of nitrogen dioxide radical.
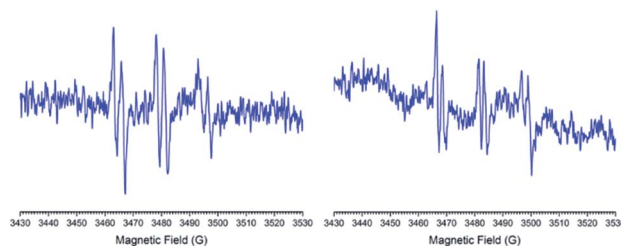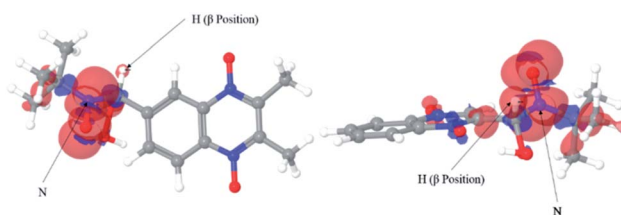

Fig. 11 Spin density isosurface for $\cdot$**nitrone 2**–OOH spin adducts using DFT calculus. The experimental spectra correspond to a delocalization of the spin density over the atoms indicated with arrows.
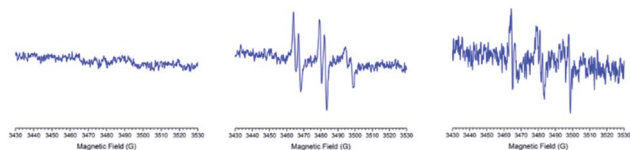
Fig. 12 (Left) The ESR-spectrum obtained in the absence of NI. Center: the ESR-spectrum obtained when nitrone 2 traps exclusively hydroxyl free radical produced by NI in the presence of mouse mammary adenocarcinoma TA3 cells. (Right) The ESR-spectrum obtained when FxBN was used in the same biological system. Both spectra were presented in the same conditions.

the **nitrone 1** was not able to trap this radical. Instead, the **nitrones 2** and **3** showed similar hyperfine patterns for this radical trapping. Fig. 10 shows the experimental spectra of the hyperfine patterns displayed by **nitrones 2** and **3**. Hyperfine coupling constants for **nitrones 2** and **3** are summarized in Table 5.

In order to corroborate the obtained spectra, we made the computational calculations for the ˙nitrone–OOH spin adduct for **nitrone 2** and **3**. In Fig. 11, it is observed that the spin densities were located mainly between the nitrogen atom and the hydrogen atom located in β-position from the nitrone group.

In this sense, the theoretical results confirm that the experimental spectra correspond to the trapping of the superoxide anion radical.

Spin trapping in biological systems studies

As it was described in our previous work,[15] the new nitrones were tested in biological models to corroborate their trapping capacity. We used mouse mammary adenocarcinoma TA3 cells and a nitroindazole (NI, 5-nitroindazole) derivative. The main characteristic of this nitro derivative is its capability to be a substrate of nitroreductases and undergoing a reduction in the presence of oxygen by one or two-electron transfer mechanism.[39] The mono electronic reductions catalyzed by nitroreductases in the presence of molecular oxygen generate superoxide anion radical, and the nitro compounds are regenerated to their initial state. This redox cycle can cause oxidative stress due to the production of superoxide anion radical. Finally, the superoxide anion radical decays to hydroxyl radical, which may trap by using spin traps. Our results showed that **nitrone 1** was not able to trap any free radicals in this model. Instead, **nitrones 2** and **3** showed sharp spectra (Fig. 12).

The analysis of the hyperfine coupling constant points out that the radical trapped corresponds to hydroxyl generated by the NI. Additionally, as Fig. 12 shows, **nitrone 2** was more sensitive to hydroxyl radical trapping in this biological model than **FxBN**.

Conclusions

New heteroaryl nitrones (**1**, **2**, and **3**) were designed, synthesized and analyzed for their ability to act as spin-trapping agents. These heteroaryl nitrones exhibit a high capacity to trap and

stabilize O-, C-, S-, and N-centered radicals. **Nitrone 1** showed different ESR-spectra, and the hyperfine coupling constant allows us to distinguish the different radicals trapped easily, but with lower half-life compared to **nitrone 2** and **3**. On the other hand, **nitrone 2** and **3** showed better spin traps capabilities due to the high stability of the spin adduct formed. In some cases, it was not so easy to distinguish the radical trapped using **nitrones 2** and **3** (specifically hydroxyl and methyl radicals), but the *g* value helped us to differentiate the trapped species. We found that these new nitrones were capable of trapping superoxide anion radical generated using xanthine/xanthine oxidase couple. Thus, we performed the trap of nitric oxide radical, in which the results obtained showed that these new nitrones are not capable of trapping this radical, but they can trap nitrogen dioxide radicals. In aqueous solution, we found that **nitrones 2** and **3** can form a spin adduct with hydroxyl radical. The half-life for these spins adducts shows a value higher than two hours. In the competition assays, the results indicated that these new nitrones (**2** and **3**) are more sensitive than DMPO to trap hydroxyl free radicals. Computational calculations supported the experimental data and allowed us to explain the different phenomena observed in this study.

Conflicts of interest

There are no conflicts to declare.

Acknowledgements

Notes and references

1 T. Finkel and N. J. Holbrook, *Nature*, 2000, **408**, 239–247.
2 J. M. Gutteridge and B. Halliwell, *Ann. N. Y. Acad. Sci.*, 2000, **899**, 136–147.
3 F. A. Villamena and J. L. Zweier, *Antioxid. Redox Signaling*, 2004, **6**, 619–629.
4 C. Olea-Azar, C. Rigol, F. Mendizabal and R. Briones, *Mini-Rev. Med. Chem.*, 2006, **6**, 211–220.
5 E. G. Janzen and J. I. P. Liu, *J. Magn. Reson.*, 1969, **9**, 510–512.
6 G. S. Timmins, K. J. Liu, E. J. Bechara, Y. Kotake and H. M. Swartz, *Free Radical Biol. Med.*, 1999, **27**, 329–333.
7 Y. Kotake and E. G. Janzen, *J. Am. Chem. Soc.*, 1991, **113**, 9503–9506.

8 R. A. Floyd, K. Hensley, M. J. Forster, J. A. Kelleher-Andersson and P. L. Wood, *Mech. Ageing Dev.*, 2002, **123**, 1021–1031.

9 G. Olive, A. Mercier, F. Le Moigne, A. Rockenbauer and P. Tordo, *Free Radicals Biol. Med.*, 2000, **28**, 403–408.

10 H. Zhao, J. Joseph, H. Zhang, H. Karoui and B. Kalyanaraman, *Free Radical Biol. Med.*, 2001, **31**, 599–606.

11 S. E. Bottle and A. S. Micallef, *Org. Biomol. Chem.*, 2003, **1**, 2581–2584.

12 S. E. Bottle, G. R. Hanson and A. S. Micallef, *Org. Biomol. Chem.*, 2003, **1**, 2585–2589.

13 B. Hatano, H. Sato, T. Ito and T. Ogata, *Synlett*, 2007, **2007**, 2130–2132.

14 B. Hatano, K. Miyoshi, H. Sato, T. Ito, T. Ogata and T. Kijima, *Tetrahedron Lett.*, 2010, **51**, 5399–5401.

15 G. Barriga, C. Olea-Azar, E. Norambuena, A. Castro, W. Porcal, A. Gerpe, M. González and H. Cerecetto, *Bioorg. Med. Chem.*, 2010, **18**, 795–802.

16 K. Sakurai, D. A. Stoyanovsky, Y. Fujimoto and A. I. Cederbaum, *Free Radical Biol. Med.*, 2000, **28**, 273–280.

17 K. Stolze, N. Udilova and H. Nohl, *Free Radicals Biol. Med.*, 2000, **29**, 1005–1014.

18 L. A. Shinobu, S. G. Jones and M. M. Jones, *Acta Pharmacol. Toxicol.*, 1984, **54**, 189–194.

19 D. R. Duling, *J. Magn. Reson., Ser. B*, 1994, **104**, 105–110.

20 M. Kamibayashi, S. Oowada, H. Kameda, T. Okada, O. Inanami, S. Ohta, T. Ozawa, K. Makino and Y. Kotake, *Free Radical Res.*, 2006, **40**, 1166–1172.

21 Y. Sueishi, C. Yoshioka, C. Olea-Azar, L. A. Reinke and Y. Kotake, *Bull. Chem. Soc. Jpn.*, 2002, **75**, 2043–2047.

22 E. Finkelstein, G. M. Rosen and E. J. Rauckman, *J. Am. Chem. Soc.*, 1980, **102**, 4994–4999.

23 C. Olea-Azar, C. Rigol, L. Opazo, A. Morello, J. D. Maya, Y. Repetto, G. Aguirre, H. Cerecetto, R. Di Maio, M. González and W. Porca, *J. Chil. Chem. Soc.*, 2003, **48**, 77–79.

24 *Density functional methods in chemistry*, ed. J. K. Labanowski and J. W. Andzelm, Springer-Verlag New York, Inc., 1991.

25 J.-L. Calais, *Int. J. Quantum Chem.*, 1993, **47**, 101.

26 A. D. Bochevarov, E. Harder, T. F. Hughes, J. R. Greenwood, D. A. Braden, D. M. Philipp, D. Rinaldo, M. D. Halls, J. Zhang and R. A. Friesner, *Int. J. Quantum Chem.*, 2013, **113**, 2110–2142.

27 J. Tomasi and M. Persico, *Chem. Rev.*, 1994, **94**, 2027–2094.

28 M. Cossi, V. Barone, R. Cammi and J. Tomasi, *Chem. Phys. Lett.*, 1996, **255**, 327–335.

29 V. Barone, M. Cossi and J. Tomasi, *J. Comput. Chem.*, 1998, **19**, 404–417.

30 W. Porcal, P. Hernandez, M. Gonzalez, A. Ferreira, C. Olea-Azar, H. Cerecetto and A. Castro, *J. Med. Chem.*, 2008, **51**, 6150–6159.

31 H. Cerecetto, E. Dias, R. Di Maio, M. Gonzalez, S. Pacce, P. Saenz, G. Seoane, L. Suescun, A. Mombru, G. Fernandez, M. Lema and J. Villalba, *J. Agric. Food Chem.*, 2000, **48**, 2995–3002.

32 C. H. Issidorides and M. J. Haddadin, Novel process for the synthesis of quinoxaline and benzimidazole-N-oxides, *US Pat.* US4866175A, 1989.

33 P. R. Marriott, M. J. Perkins and D. Griller, *Can. J. Chem.*, 1980, **58**, 803–807.

34 A. J. Carmichael, K. Makino and P. Riesz, *Radiat. Res.*, 1984, **100**, 222–234.

35 R. Sridhar, P. Beaumont and E. Powers, *J. Radioanal. Nucl. Chem.*, 1986, **101**, 227–237.

36 S. Goldstein and P. Lestage, *Curr. Med. Chem.*, 2000, **7**, 1255–1267.

37 S. Pou, L. Keaton, W. Surichamorn, P. Frigillana and G. M. Rosen, *Biochim. Biophys. Acta*, 1994, **1201**, 118–124.

38 K. J. Reszka, P. Bilski and C. F. Chignell, *Nitric Oxide*, 2004, **10**, 53–59.

39 D. W. Bryant, D. R. McCalla, M. Leeksma and P. Laneuville, *Can. J. Microbiol.*, 1981, **27**, 81–86.